Electronic Supplementary Material (ESI) for Nanoscale.

Stochastic vs. deterministic magnetic coding in designed cylindrical nanowires for 3D magnetic networks

Cristina Bran[1], Elias Saugar[1], Jose Angel Fernandez-Roldan[1,2], Rafael P. del Real[1], Agustina Asenjo[1], Lucia Aballe[3], Michael Foerster[3], Arantxa Fraile Rodríguez[4,5], Ester M. Palmero[1,6], Manuel Vazquez[1] and Oksana Chubykalo-Fesenko[1]

[1] Instituto de Ciencia de Materiales de Madrid, CSIC, Madrid, 28049, Spain
[2] Department of Physics, University of Oviedo, Oviedo, 33007, Spain
[3] ALBA Synchrotron Light Facility, CELLS, Barcelona, 08290, Spain
[4] Departament de Física de la Matèria Condensada, Universitat de Barcelona, Barcelona, 08028, Spain
[5] Institut de Nanociència i Nanotecnologia (IN2UB), Universitat de Barcelona, Barcelona, 08028, Spain
[6]Group of Permanent Magnets and Applications, IMDEA Nanoscience, Madrid, 28049, Spain

SUPPLEMENTARY INFORMATION

XMCD-PEEM

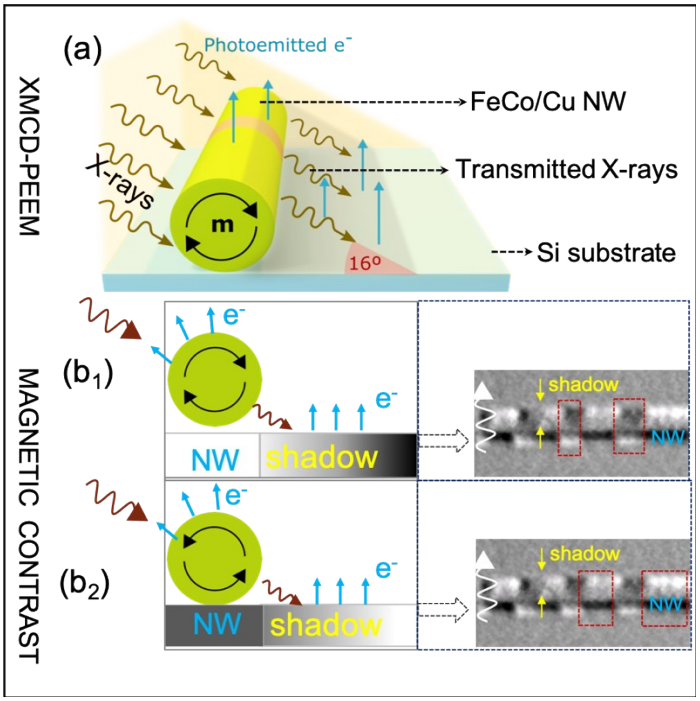

Figure S1. Schematic illustrations of (a) the principle of the dual sensitivity of Photoemission Electron Microscopy (PEEM) to detect direct photoemission and transmission data using X-ray Magnetic Circular Dichroism (XMCD) as a contrast mechanism, (b) magnetic contrast observed for direct photoemission and transmission for vortices oriented parallel (b_1) and antiparallel (b_2) to the x-ray beam. The insets (right side) in (b1)-(b2) show examples of a XMCD-PEEM image of a FeCo/Cu NW with vortices (dashed red squares) oriented parallel (bright contrast on the NW, dark in the shadow) and antiparallel (dark contrast on the NW and

bright in the shadow) to the x-ray beam. The wriggle arrows in (a) and (b) depict the x-rays. The nanowire (NW) and shadow are marked in blue and yellow, respectively in the XMCD-PEEM image.

Figure S1 shows a schematic view of XMCD-PEEM contrasts formed on the nanowire (NW) and shadow. The nanowire is illuminated with circularly polarized X-rays at a grazing angle of 16º with respect to the surface (Fig. S1-a), at the resonant L_3 absorption edge of Co (778 eV).

The images are the projection of the local magnetization on the photon propagation vector so that ferromagnetic domains with magnetic moments parallel (Fig. S1-b1) or antiparallel (Fig. S1-b2) to the X-ray propagation vector appear bright or dark in the XMCD image while domains with magnetic moments at a different angle have an intermediate gray contrast. The particular cylindrical shape of the wires allows for a fractional part of X-rays to be transmitted through the nanowire, generating photoemission from the Si substrate. By analyzing the circular dichroic or pseudo-magnetic contrast formed in transmission in the shadow area, information about the magnetic configuration in the bulk of the wire can then be obtained [1-3].

The schematic case in Fig. S1(b) presents a nanowire showing vortex domains with different chirality. The bright (Fig. S1 (b1))/dark (Fig. S1 (b2)) contrast at the right-side, labelled NW, in (b1 and b2) is related to the surface magnetization of the nanowire. Notice that the bright (b1)/dark (b2) contrast in direct photoemission (left-side, labelled NW) is equivalent to the dark(b1)/bright (b2) one in transmission, labeled shadow (right-side), since the absorbed and transmitted X-rays are complementary.

Figures S1 (b1)-(b2)-insets (dotted black squares) present two examples of magnetic contrast observed in XMCD-PEEM. The dotted red square in Fig. S1 (b1)-inset shows a vortex domain oriented parallel to the x-ray beam, as sketched in Fig. S1 (b1) while Fig. S1 (b2)-inset shows a vortex domain oriented antiparallel to the x-ray beam, as sketched in Fig. S1 (b2).

Modelled hysteresis cycles

Hysteresis cycles were calculated using micromagnetic simulations with the fields applied perpendicular to the nanowire axis in two directions, see Figs. S2 and S3. Calculations indicate a small hysteresis corresponding to nucleation and annihilation of the vortex state. The saturation, nucleation and the annihilation fields are larger for the field applied in Z-direction than for the field applied in Y direction, while the hysteresis is narrower in the former case. For the field applied in Z-direction the remanent state consists of alternating vortices, while for the field applied in Y-direction a bi-vortex state is formed.

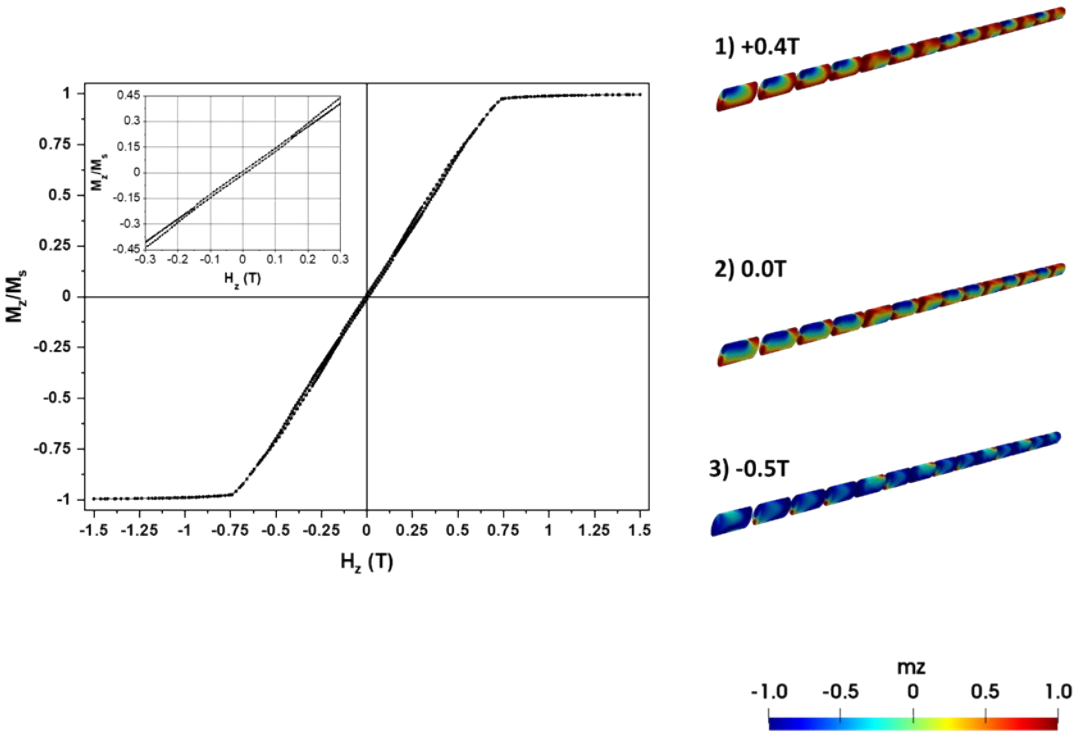

Figure S2. Simulated hysteresis with the field applied at Z-direction (left panel) and selected configurations at indicated points.

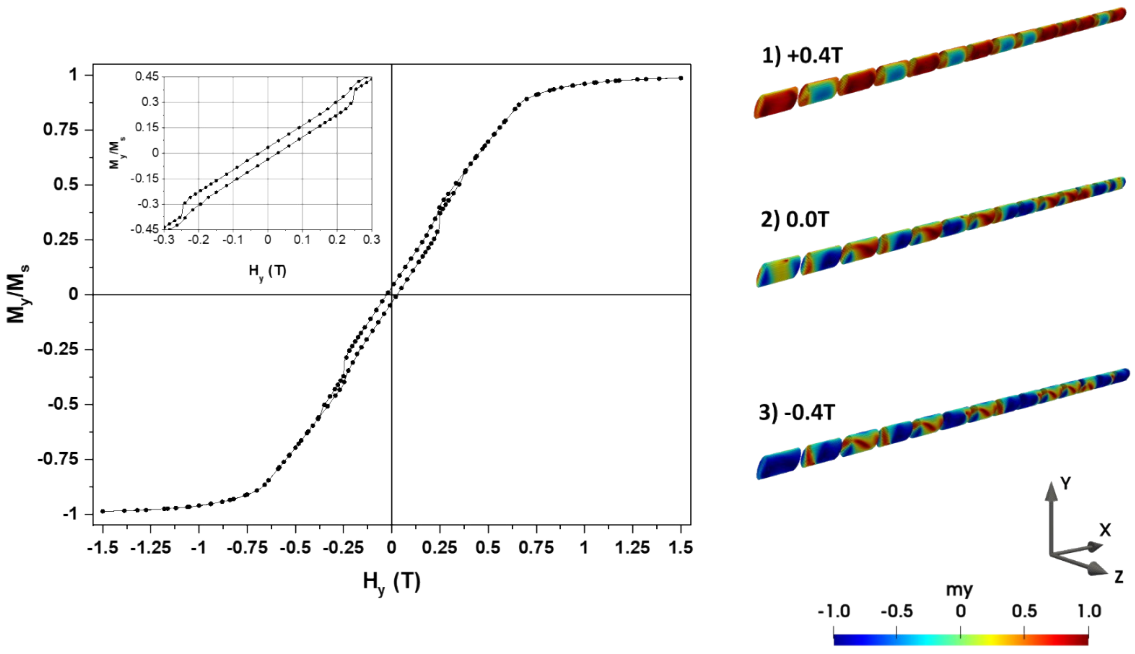

Figure S3. Simulated hysteresis with the field applied at Y-direction (left panel) and selected configurations at indicated points.

Chirality switching with different initial configurations

In the following we present different examples for random and deterministic chirality switching starting with different initial configurations: the same polarity in all segments and the same (Fig.S4) and alternating (Fig.S5) chirality. In both cases stochastic switching is observed for the field applied

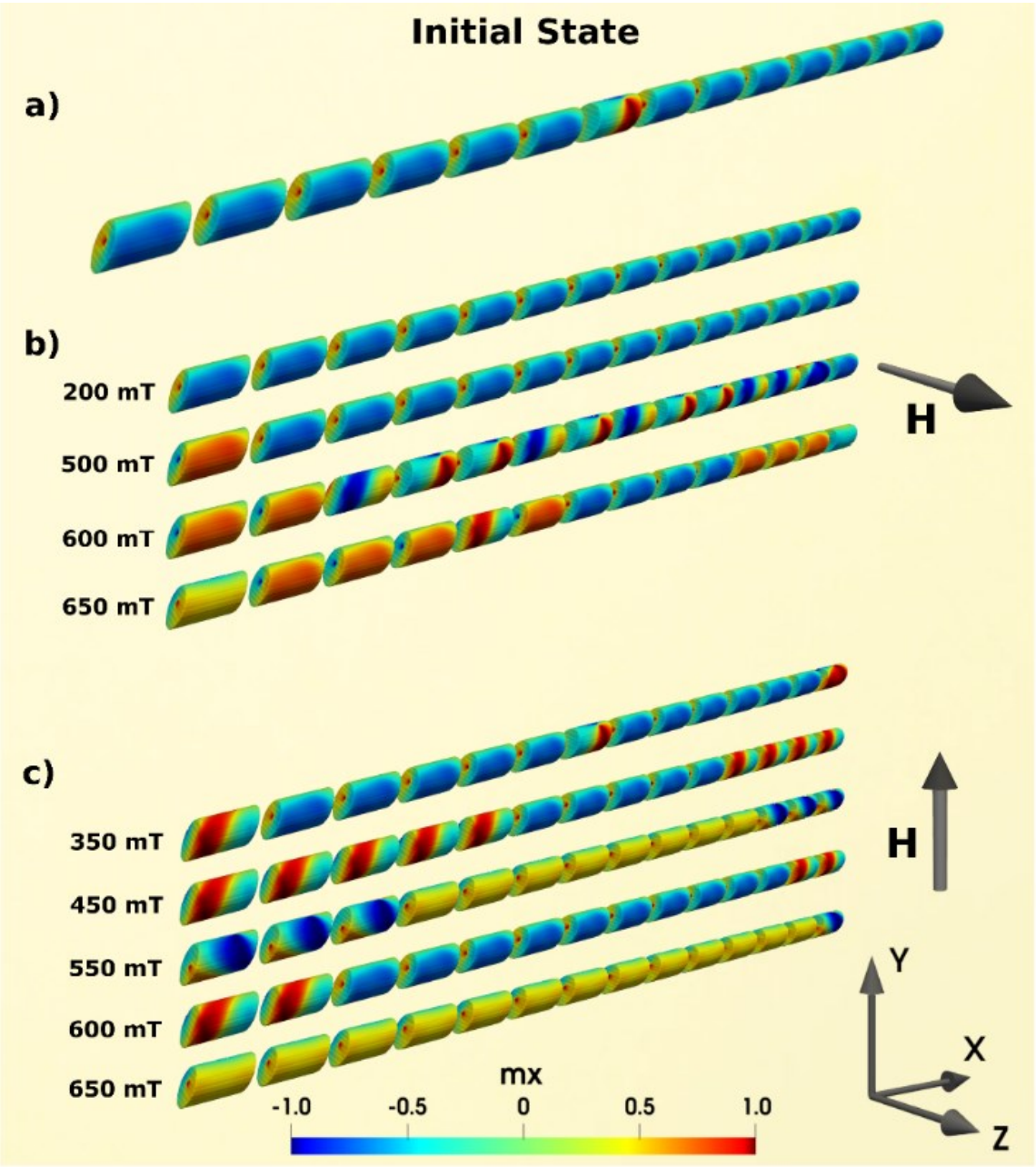

in Z-direction and the deterministic switching for the field applied in Y-direction.

Figure S4. Micromagnetic modelling with the initial state (a) having the same polarity and chirality of vortices in all segments showing (b) random chirality switching with the field applied in Z-direction and (c) deterministic chirality switching with the field applied in Y-direction.

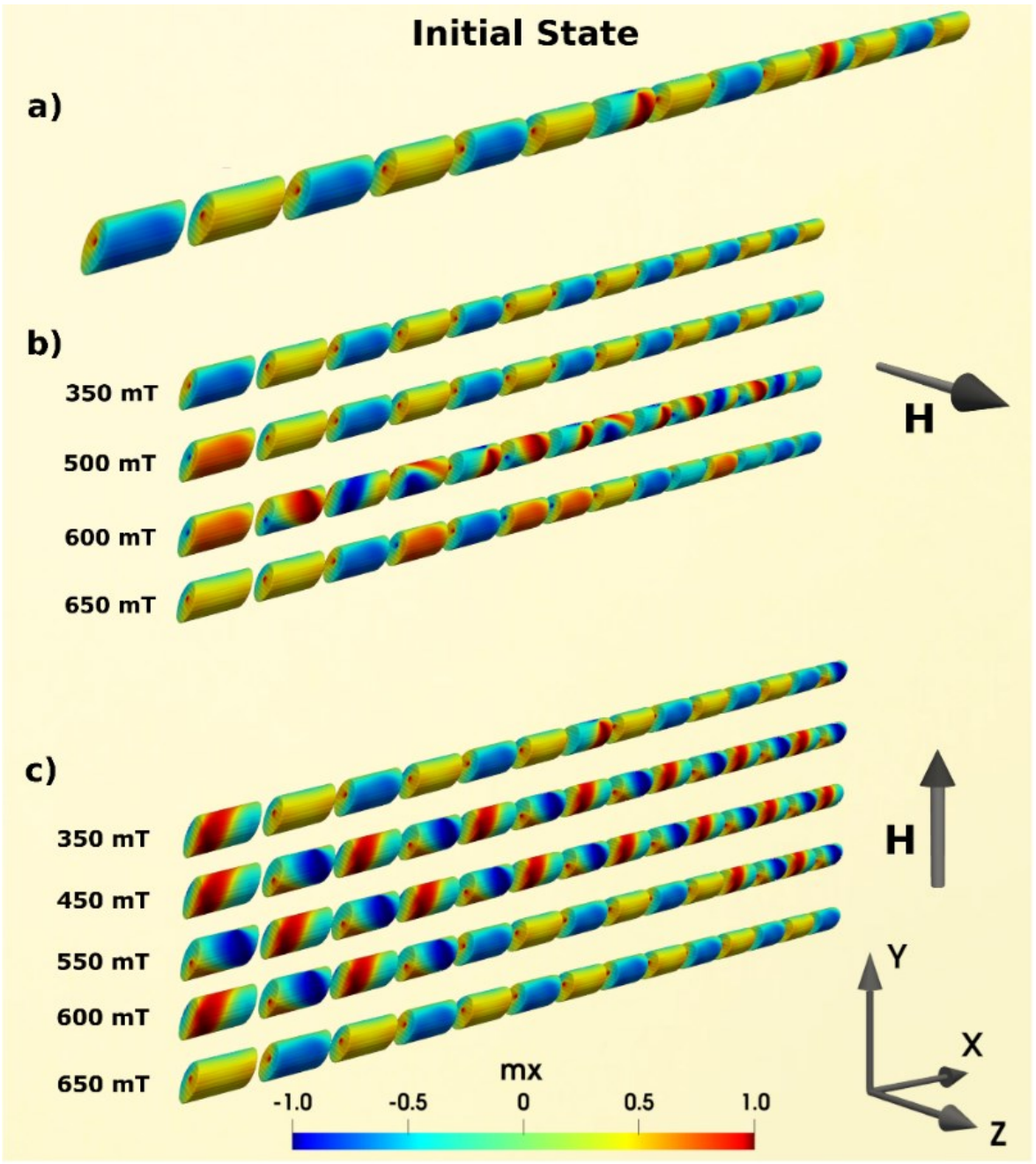

Figure S5. Micromagnetic modelling with the initial state (a) having the same polarity and alternating vortex chirality in all segments showing (b) random chirality switching with the field applied in Z-direction and (c) deterministic chirality switching with the field applied in Y-direction.

Polarity switching

The minimum energy configuration corresponds to a situation when all vortex cores are parallel to the nanowire axis. However, as it is observed in Figs. S4b and S5b application of the field in Z-direction changes the vortex cores in arbitrary directions. Note that this situation is not favorable from the point of view of the magnetostatic energy minimization and we do not expect it as an initial state in our experiment. Interestingly, next application of the field in Y direction aligns again the cores. In Fig.S6 we present results of the micromagnetic modelling where we start with the initial state corresponding to both arbitrary chirality and polarity pattern. After applying the field in Y direction, we observe that all vortex cores are aligned along +X direction, Note that the chirality is switched to the opposite in many (but not all) segments for this field values.

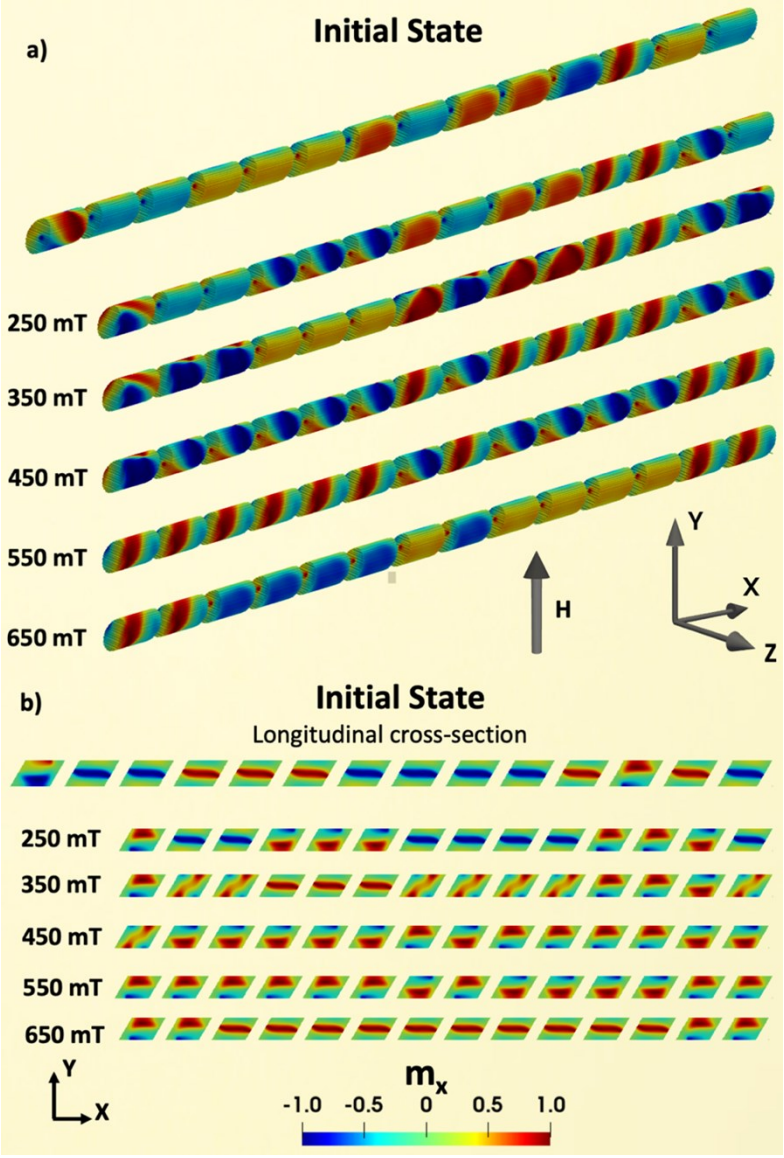

Figure S6. Micromagnetic modelling with the initial state represented in (a), upper image, having an arbitrary chirality and polarity pattern. After the application of field sequences in Y directions all cores are aligned parallel to the nanowire axis while the chirality are switched to the opposite to the initial state in many segments. Images in (b) represent longitudinal cross sections demonstrating the final vortex core alignment.

Chirality switching with 45 degrees tilting angle and smaller non-magnetic spacing

In the following we present different examples for random and deterministic chirality switching. To demonstrate a general nature of our results we model a multilayered nanowire with a decreased non-magnetic spacing down to 30 nm and a larger tilting angle of 45 degrees. The modelling starts with the same initial configuration, presented in panel (Fig.S7 a), a random vortex chirality and the same polarities. The stochastic switching is observed for the field applied in Z-direction and the deterministic switching for the field applied in Y-direction.

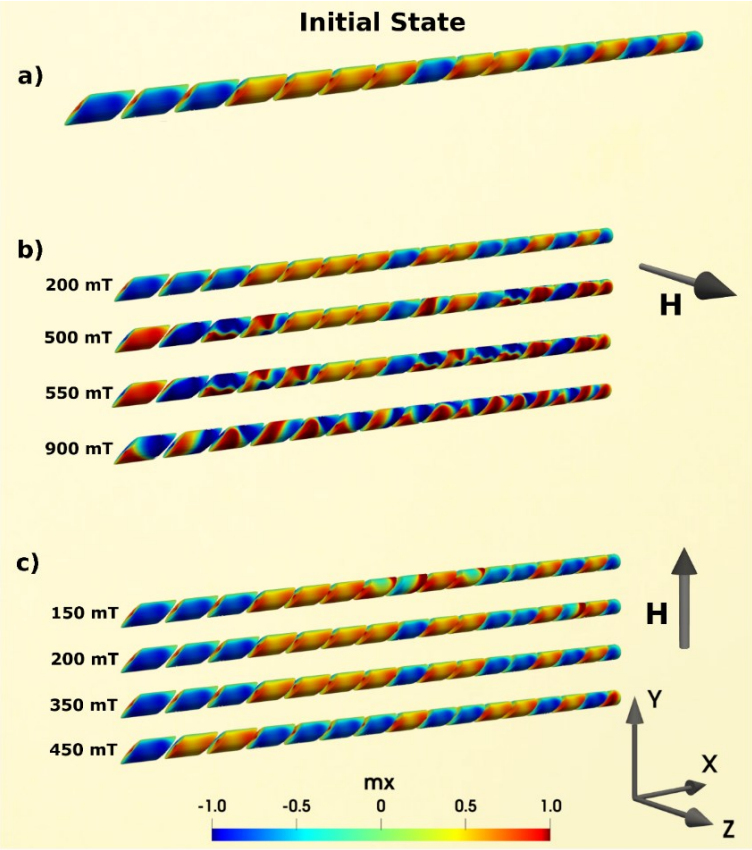

Figure S7. Micromagnetic modelling of a multilayered nanowire with 30 nm non-magnetic spacing and 45 degrees tilting angle. (a) the initial state having random vortex chirality with the same polarities in all segments showing (b) random chirality switching with the field applied in Z-direction and (c) deterministic chirality switching with the field applied in Y-direction.

Comparatively to the results presented in the main text, the deterministic switching required a smaller field while the stochastic one – a much larger field magnitude. Additionally, different remanent states were created in the case of stochastic switching. These configurations are presented in Fig. S8. After applying 550 mT field in Z direction some segments appeared in the three-vortex state, as illustrated in Fig.S8b where one vortex is placed in the segment center with the core pointing perpendicular to the nanowire surface and two vortices are formed at the segment ends with the cores pointing along the nanowire axis. After a subsequent application of larger fields, the three-vortex states were converted either into a one-vortex or a two-vortex states, see Fig.S8. The one-vortex state may have a curvilinear vortex core going from the segment center towards its surface as in Fig.S8d. The two-vortex state is characterized by two repelling vortex cores going from the segment center towards its surface in the opposite directions, as presented in Fig.S8e.

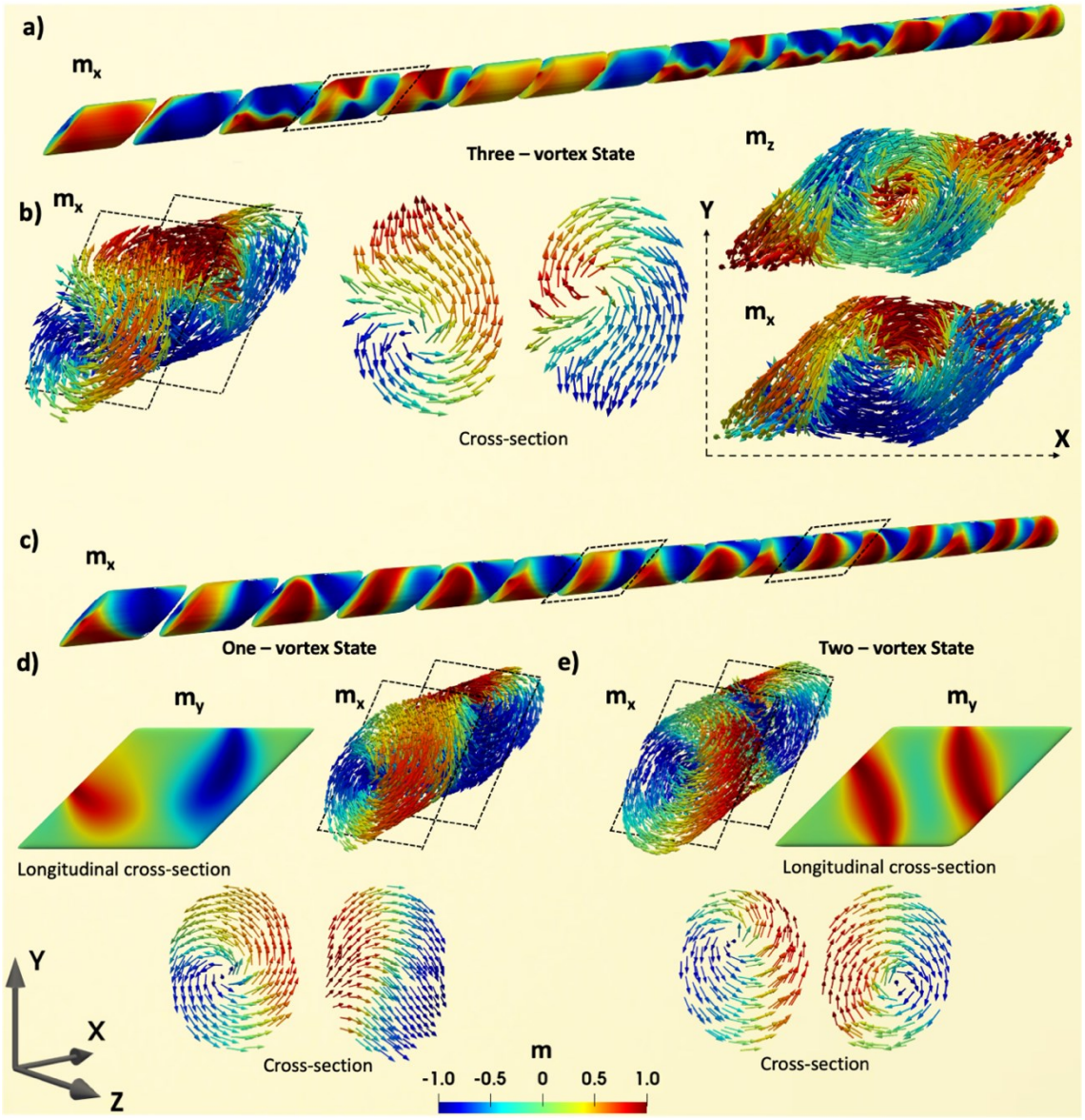

Figure S8. (a) Remanent state after applying 550 mT in Z direction corresponding to initial configuration and field sequences of Fig.S7 (b). Three-vortex configuration of the marked segment in S8(a) and its transverse and longitudinal cross-sections. c) Remanent state after applying 900mT in Z direction (d) and (e) represent magnetization states of selected segments and their longitudinal and transverse cross-sections (d) a one-vortex state with the vortex core going along the diagonal and (e) a two-vortex state with two repelling cores.

Evolution of the magnetic configurations

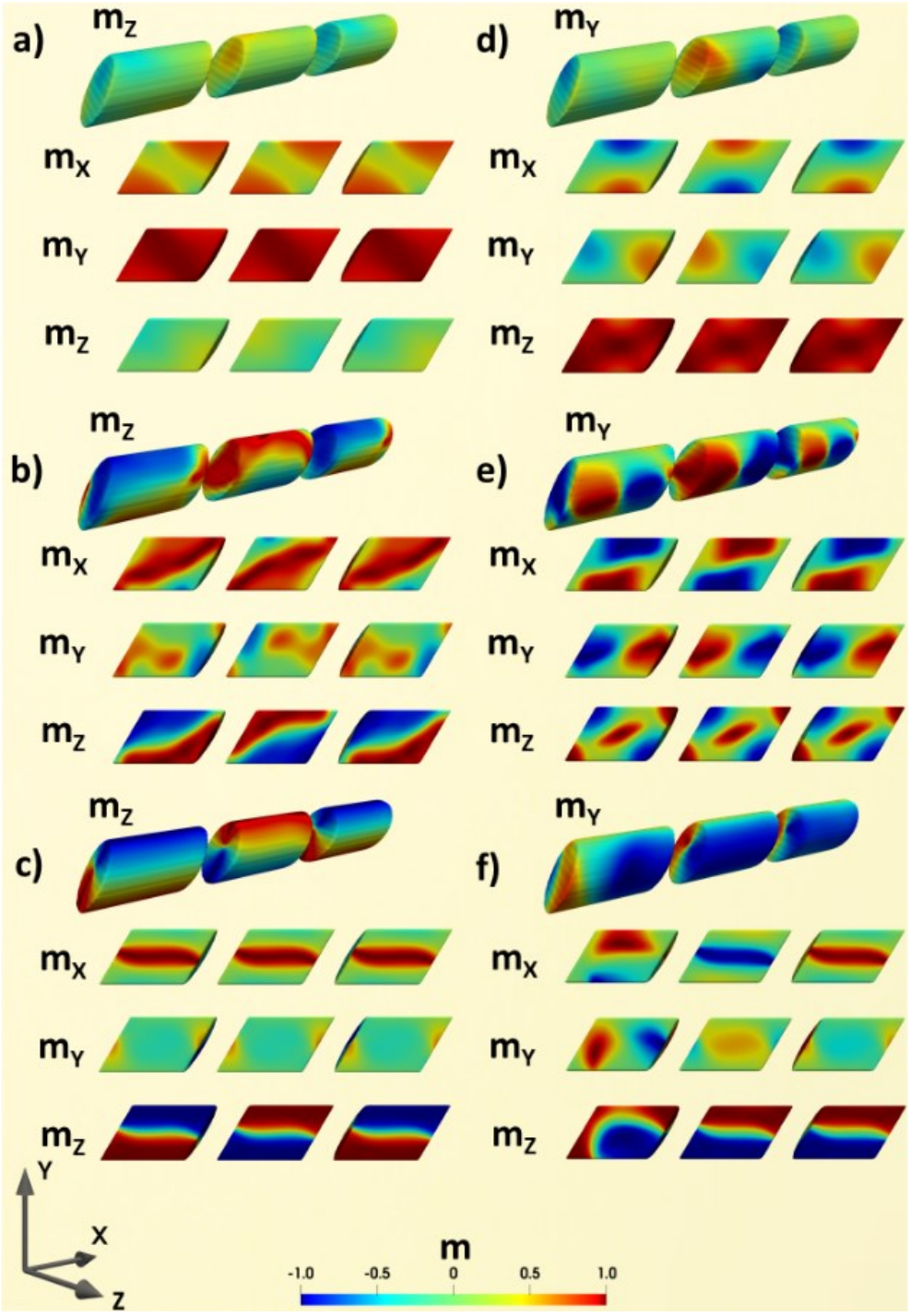

Figure S9. Modelled evolution of the magnetization configurations for critical field 650 mT applied field in both perpendicular to the nanowire axis directions. For states (a) – (c) the field is applied in Y direction. For states (d)-(f) the field is applied in Z direction. Below each 3D image, longitudinal cross-sections are shown with 3 components of magnetization.

References:

1. Scholl, A.; Ohldag, H.; Nolting, F.; Stöhr, J.; Padmore, H.A. X-ray photoemission electron microscopy, a tool for the investigation of complex magnetic structures (invited). *Rev. Sci. Instrum.* **2002**, *73*, 1362–1366, doi:10.1063/1.1445485.

2. Kimling, J.; Kronast, F.; Martens, S.; Böhnert, T.; Martens, M.; Herrero-Albillos, J.; Tati-Bismaths, L.; Merkt, U.; Nielsch, K.; Meier, G. Photoemission electron microscopy of three-dimensional magnetization configurations in core-shell nanostructures. *Phys. Rev. B - Condens. Matter Mater. Phys.* **2011**, *84*, doi:10.1103/PhysRevB.84.174406.

3. Bran, C.; Berganza, E.; Palmero, E.M.; Fernandez-Roldan, J.A.; Del Real, R.P.; Aballe, L.; Foerster, M.; Asenjo, A.; Fraile Rodríguez, A.; Vazquez, M. Spin configuration of cylindrical bamboo-like magnetic nanowires. *J. Mater. Chem. C* **2016**, *4*, 978–984, doi:10.1039/C5TC04194E.